Properties of inductively coupled rf Ar/H_2 plasmas: Experiment and global model

Takashi Kimura[a] and Hiroki Kasugai
Graduate School of Engineering, Nagoya Institute of Technology, Nagoya 466-8555, Japan

(Received 16 December 2009; accepted 2 February 2010; published online 29 April 2010)

Experiments with a Langmuir probe and optical emission spectroscopy combined with actinometry are carried out in inductively coupled rf (13.56 MHz) Ar/H_2 discharges at total pressures of 20 m, 40 m, and 60 mTorr in hydrogen fractions ranging from 0% to 50%. The measured electron energy probability functions (EEPFs), which deviate from the Maxwellian distributions owing to the depletion of high-energy electrons, can be approximated using two temperatures. The electron temperatures, which can be deduced from the slopes of low-energy and high-energy parts of the EEPFs, relatively abruptly increase with increasing the hydrogen fraction in the hydrogen fractions below 10%, whereas the measured electron density markedly decreases with increasing the hydrogen fraction in the hydrogen fractions below 20%. The effective ion mass, which can be estimated from the ion current collected into the probe, markedly decreases with increasing the hydrogen fraction. The density of hydrogen atoms estimated by actinometry markedly increases as molecular hydrogen is added to Ar discharges, and then gradually increases with increasing the hydrogen fraction at the hydrogen fractions higher than 10%–20%. A global model is used to study the effect of Ar dilution to hydrogen discharges on the plasma parameters assuming the Maxwellian electron energy distribution. The model results are compared with the experimental results, obtaining reasonably good agreement. © *2010 American Institute of Physics*.
[doi:10.1063/1.3345084]

I. INTRODUCTION

Hydrogen containing discharges are widely used in various industrial applications, such as etching processes, reduction in oxides on surfaces, surface passivation, and film deposition.[1–5] For example, the discharges of hydrogen in a mixture with silane or hydrocarbons are used in order to produce the precursors for the plasma assisted deposition of microcrystalline silicon thin films or diamond synthesis, respectively.[4–7] Recently, various surface treatments of SiCOH-type films by exposure to hydrogen plasmas have been investigated.[8] In these applications, the active species, such as hydrogen atoms and hydrogen ions, should be responsible for surface reactions in various processes, and the hydrogen containing discharges with a high dissociation rate are required as sources of such active species. Therefore, the degree of dissociation of molecular hydrogen is considered as one of the most important parameters of hydrogen containing plasmas.[9–11] Low-pressure and high-density plasmas, which have been produced in inductively and capacitively coupled discharges and electron cyclotron resonance discharges, are used in order to achieve the high densities of such active species. Inductively coupled discharges, which are typically operated at pressures lower than 50–60 mTorr in typical electron density range of 10^{16}–10^{18} m^{-3}, have been widely used in the material processing because the plasma density and the ion bombarding energy at the surface can be independently controlled. In practice, density of hydrogen atoms and the degree of dissociation in such plasmas have been measured using optical emission and laser spectroscopy.[11]

Hydrogen plasmas produced in various types of discharges have been studied for many years. Earlier on, theoretical investigations on hydrogen plasmas were conducted in wide pressure range higher than hundreds of millitorr, focusing on their important kinetic description.[12–18] Although the physical and chemical processes in the hydrogen plasmas have been revealed through these investigations, the differences in the operating conditions, such as the pressure and power injected into plasmas, may cause different behaviors in the plasma chemistry. Recently, the properties of capacitively-coupled and inductively-coupled hydrogen discharges have been investigated.[19–22] The global model, which was developed by Lieberman and Gottscho[23] for noble gases and extended to molecular gases by Lee *et al.*,[24,25] is one of the methods that have been used in order to treat the physical and chemical processes in the plasmas. The addition of Ar to the hydrogen discharges may cause a change in the shape of the electron energy distribution, which can induce the change in the rate coefficients related to electron-induced inelastic collision processes, and an increase in electron density. In addition, interactions, such as quenching collisions between excited Ar and molecular hydrogen, and charge exchange collisions between Ar ions and the molecular hydrogen, can play a significant role on the determination of plasma compositions.[26,27] In order to understand the behavior of Ar/H_2 plasmas, significant reactions among the reactive

[a]Electronic mail: t-kimura@nitech.ac.jp.

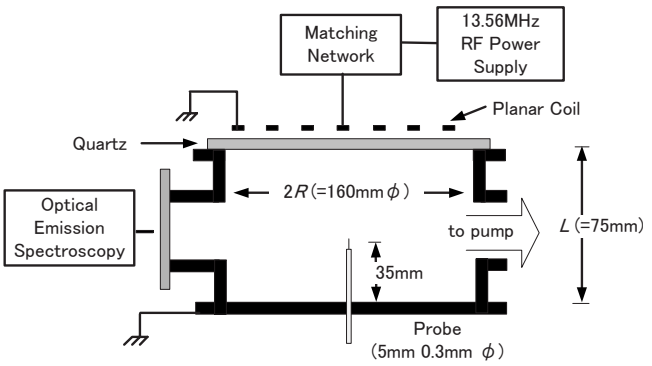

FIG. 1. Schematic diagram of experimental set-up.

species in the discharge, electrons, ions, and atoms must be taken into account, including the effects of the plasma-wall interactions.

The objectives of this research are to investigate the effect of argon dilution on plasma parameters in inductively-coupled rf (13.56 MHz) Ar/H_2 discharges and to understand the plasma chemistry of such discharges using the global model. In this paper, the plasma parameters in low-pressure inductively-coupled Ar/H_2 discharges are first investigated as a function of hydrogen fraction. Second, the global model for finite cylindrical discharges is applied in order to understand the plasma chemistry of Ar/H_2 discharges, and the model results are compared with some experimental values.

II. EXPERIMENTAL PROCEDURE

A schematic diagram of the experimental apparatus is shown in Fig. 1. The stainless steel chamber is cylindrical, 160 mm in inner diameter and 75 mm in length, with a quartz plate of 10 mm thickness placed at the upper end of the chamber. The rf discharges are sustained by an azimuthal electric field induced by a rf coil current supplied to a planar three-turn coil from a power source connected to an L-type capacitive matching network. The planar coil mounted about 5 mm above the quartz plate is concentric in the center of the chamber to maintain the discharge symmetry. An electrostatic shield can practically eliminate the capacitive coupling between the coil and the plasma, resulting in suppression of any rf plasma potential fluctuation. A cylindrical probe 5 mm in length and 0.3 mm in diameter is installed at the chamber center. The power P_{abs} injected into the plasma, which is estimated by subtracting the transmitted power without plasma from that with plasma at the same current, is kept at 120 W in our experiment. The flow rates of Ar and H_2 are controlled using two mass-flow controllers, and the total flow rate corresponding to the sum of two flow rates is maintained at about 30–40 SCCM (SCCM denotes cubic centimeter per minute at STP). Here, the H_2 fraction δ_{H_2} corresponds to the ratio of the partial pressure of H_2 to the total pressure p.

The electron energy distribution function (EEDF) $F(\varepsilon)$ can be measured by detecting the second derivative i_p'' of the probe current i_p with respect to the probe bias voltage V_p,[28]

$$F(\varepsilon) = \frac{4}{Ae^2}\left(\frac{m}{2e}\right)^{1/2} V^{1/2} i_p'', \tag{1}$$

where ε is the electron energy in electronvolt, A the probe area, e the absolute value of electron charge, m the electron mass, and V the voltage difference between the plasma potential, which is determined as the bias voltage corresponding to $i_p''=0$ and V_p. The measured electron energy probability function (EEPF) $f(\varepsilon)$ can then be deduced as

$$f(\varepsilon) = F(\varepsilon)\varepsilon^{-1/2}. \tag{2}$$

The EEDF detection system is described in a previously published paper.[29] The electron density n_e and the effective electron temperature T_{eff}, which are calculated using the measured EEPF, are given as follows:

$$n_e = \int_0^\infty \varepsilon^{1/2} f(\varepsilon) d\varepsilon, \tag{3}$$

$$T_{eff} = \frac{2}{3}\bar{\varepsilon} = \frac{2}{3n_e}\int_0^\infty \varepsilon^{3/2} f(\varepsilon) d\varepsilon. \tag{4}$$

In order to grasp the variation in the dominant ion species with varying the hydrogen fraction, the effective ion mass is estimated by the ion current collected into the probe. The ion current $I_i(V)$ collected into the cylindrical probe can be approximated as

$$I_i(V) \approx eA \sum n_{is(X)} \left(\frac{T_{eff}}{M_{i(X)}}\right)^{1/2} \left(1 + \frac{eV}{T_{eff}}\right)^{1/2}, \tag{5}$$

where $n_{is(X)}$ is the density of ion species X (X=Ar, H, H_2, H_3, and ArH) at the probe sheath edge and $M_{i(X)}$ is the ion mass of ion species X. In the case that the voltage difference V is much larger than T_{eff}/e, the ion current $I_i(V)$ is given by

$$I_i(V) \approx eA \sum n_{is(X)} \left(\frac{eV}{M_{i(X)}}\right)^{1/2}. \tag{6}$$

The effective ion mass M_{eff} is defined as

$$\left(\frac{1}{M_{eff}}\right)^{1/2} \approx \frac{\Sigma n_{is(X)} M_{i(X)}^{-1/2}}{\Sigma n_{is(X)}}. \tag{7}$$

Moreover we define h_{pr} as the ratio of the total ion density at the probe sheath edge to the electron density at the bulk plasma, and then the mass M_{eff} is given as

$$M_{eff} \approx \left[\frac{eAh_{pr}n_e}{I_i(V)}\right]^2 eV. \tag{8}$$

The value of h_{pr} should be experimentally determined using n_e and $I_i(V)$ at $V=40$ V measured in pure Ar discharges in order to satisfy $M_{eff}=40$, and the value of M_{eff} at each experiment should be deduced using h_{pr}, n_e, and $I_i(V)$ at $V=40$ V.

Optical emission spectroscopy is carried out in order to obtain the relationship between the hydrogen fraction and the density of ground-state hydrogen atoms. The density of hydrogen atoms in the plasmas is estimated from the optical emission intensities at 485.6 nm (H_β line) and 750.4 nm (the excited Ar) (Ref. 11) because the excitation cross sections of

the hydrogen atoms and Ar have similar energy dependence. However, the density of molecular hydrogens in low-temperature hydrogen containing plasmas is much larger than that of hydrogen atoms. Therefore, the optical emission intensity at 485.6 nm emitted through the dissociative-excitation process of molecular hydrogen must be considered since it often yields a very important contribution. The optical emission intensities I_{486} and I_{750} at 485.6 and 750.4 nm are approximately given as

$$I_{486} \approx C_{i,j(\mathrm{H})} h\nu_{i,j(\mathrm{H})} \frac{A_{i,j(\mathrm{H})}}{\Sigma A_{i,j(\mathrm{H})}} n_e (k_{\mathrm{exc,H}} n_{\mathrm{H}} + k_{\mathrm{dis\text{-}exc,H_2}} n_{\mathrm{H_2}}),$$

$$I_{750} \approx C_{i,j(\mathrm{Ar})} h\nu_{i,j(\mathrm{Ar})} n_e k_{\mathrm{exc,Ar}} n_{\mathrm{Ar}},$$

where $k_{\mathrm{exc,H}}$ and $k_{\mathrm{exc,Ar}}$ correspond to the excitation rate coefficients of the ground-state hydrogen atom and Ar, respectively, $k_{\mathrm{dis\text{-}exc,H_2}}$ the dissociative-excitation rate coefficient of the ground-state molecular hydrogen, n_{X} the density of the neutral species X (=H, H_2, and Ar), $C_{\mathrm{i,j(X)}}$ the constant related to the solid angle and spectral response of the optical system, h the Planck's constant, $\nu_{i,j(\mathrm{X})}$ the frequency of the transition from the i-level to the j-level, and $A_{i,j(\mathrm{X})}$ is the Einstein coefficient for the observed transition. The total gas density n_{g}, which can be given using the total pressure p and the gas temperature T_{g}, corresponds to $n_{\mathrm{H}}+n_{\mathrm{H_2}}+n_{\mathrm{Ar}}=n_{\mathrm{g}}$. With this relation and the measured intensity ratios, the density n_{H} of the ground-state hydrogen atoms is given as

$$n_{\mathrm{H}} = \frac{C_0 \frac{I_{486}}{I_{750}} R_{\mathrm{Ar,H}} n_{\mathrm{Ar}} - R_{\mathrm{H_2,H}} (n_{\mathrm{g}} - n_{\mathrm{Ar}})}{1 - R_{\mathrm{H_2,H}}}, \tag{9}$$

where C_0 is given as

$$C_0 = \frac{C_{i,j(\mathrm{Ar})} \nu_{i,j(\mathrm{Ar})} \Sigma A_{i,j(\mathrm{H})}}{C_{i,j(\mathrm{H})} \nu_{i,j(\mathrm{H})} A_{i,j(\mathrm{H})}},$$

and $R_{\mathrm{Ar,H}}$ and $R_{\mathrm{H_2,H}}$, which correspond to the ratio of the corresponding excitation rate coefficients, are given as $R_{\mathrm{Ar,H}}=k_{\mathrm{exc,Ar}}/k_{\mathrm{exc,H}}$ and $R_{\mathrm{H_2,H}}=k_{\mathrm{dis\text{-}exc,H_2}}/k_{\mathrm{exc,H}}$, respectively.

III. DESCRIPTION OF GLOBAL MODEL

A global model for electropositive plasma is applied to the Ar/H_2 plasmas in a cylindrical chamber of radius R and length L since the electronegativity, which corresponds to the ratio of H^- density to electron density, can be assumed to be very low. The electronegativity will be discussed at the last of this section. The reactions considered in the model are listed in Tables I–III. Eight neutral species (Ar, Ar metastables (the levels $1s^5$ and $1s^3$) Ar_m, Ar resonant [the levels $1s^4$ and $1s^2$) Ar_r, Ar excited to $4p$-state Ar($4p$), H_2, H($1s$), H($2s$), and H($2p$)] and six charged species (electrons, Ar^+, ArH^+, H^+, H_2^+, and H_3^+) in the Ar/H_2 plasmas are considered. Here, the density of Ar($4p$) atoms refers to the total of all the ten energy levels belonging to the $4p$ manifold. All neutral species are assumed to be uniform over the chamber. The dissociation reactions of H_2 by the electron impact, which correspond to $k_j(j=19-22)$, are assumed to be accomplished

TABLE I. Main reaction set for argon.

Reaction	Rate coefficient ($m^3\ s^{-1}$)	Ref.
$Ar+e \rightharpoonup Ar_m+e$	$k_1=5.0\times10^{-15}\exp(-12.64/T_e)$	32
$Ar+e \rightharpoonup Ar_r+e$	$k_2=1.9\times10^{-15}\exp(-12.6/T_e)$	32
$Ar+e \rightharpoonup Ar(4p)+e$	$k_3=2.1\times10^{-14}\exp(-13.13/T_e)$	32
$Ar+e \rightharpoonup Ar^+ +2e$	$k_4=2.3\times10^{-14}T_e^{0.59}\exp(-17.44/T_e)$	32
$Ar_m+e \rightharpoonup Ar^+ +2e$	$k_5=1\times10^{-13}\exp(-4.2/T_e)$	33 and 34
$Ar_r+e \rightharpoonup Ar^+ +2e$	$k_6=1\times10^{-13}\exp(-4.2/T_e)$	33 and 34
$Ar(4p)+e \rightharpoonup Ar^+ +2e$	$k_7=1.8\times10^{-13}T_e^{0.61}\exp(-2.61/T_e)$	32
$Ar_m+e \rightharpoonup Ar_r+e$	$k_8=3.7\times10^{-13}$	33 and 34
$Ar_m+e \rightharpoonup Ar(4p)+e$	$k_9=8.9\times10^{-13}T_e^{0.51}\exp(-1.59/T_e)$	32
$Ar_r+e \rightharpoonup Ar(4p)+e$	$k_{10}=8.9\times10^{-13}T_e^{0.51}\exp(-1.59/T_e)$	32
$Ar_r+e \rightharpoonup Ar_m+e$	$k_{11}=9.1\times10^{-13}$	32
$Ar_m+Ar_m \rightharpoonup Ar^+ +Ar+e$	$k_{12}=6\times10^{-16}$	32–34
$Ar_m+Ar_r \rightharpoonup Ar^+ +Ar+e$	$k_{13}=2.1\times10^{-15}$	32–34
$Ar_r \rightharpoonup Ar+h\nu$	τ_{rad}	33 and 34
$Ar(4p) \rightharpoonup Ar_r+h\nu$	$3\times10^7\ (s^{-1})$	32
$Ar(4p) \rightharpoonup Ar_m+h\nu$	$3\times10^7\ (s^{-1})$	32
$Ar_m \rightharpoonup Ar$ (wall loss)	$D_{\mathrm{m,Ar}}/\Lambda^2$	
$Ar^+ \rightharpoonup Ar$ (wall loss)	$Ar^+_{\mathrm{Loss}}=2U_{\mathrm{B,Ar}}(R^2h_\ell+RLh_r)/R^2L(s^{-1})$	

by a decay of the excitation of electronic states of H_2, such as $b\ ^3\Sigma_u^+$ and $a\ ^3\Sigma_g^+$, which are produced by the electron-induced inelastic collisions into atoms. Electrons which have a Maxwellian energy distribution with electron temperature T_e are also assumed to be uniform over the chamber since the plasma dimensions are approximately equal to the chamber dimensions due to the thin sheath for inductive discharges. All positive ion species, which are assumed to have the same profile, must satisfy the quasineutrality, $n_e=n_+$, where n_+ is the sum of the positive ion densities. The gas temperature in the discharge space is assumed to be 400 K because the power density in the plasma is about 0.09 W/cm^3 in our experiment.

The particle balance equation for each species is described by a set of first-order differential equations. The equation describes the creation, volumetric losses, and surface reactions. In the steady state, total production and loss rates must balance so that the time variation in each species density is equal to zero. The diffusional losses of neutral radicals to the wall are estimated by an effective loss rate. The effective loss rate X_{Loss} for a radical X is given by

$$X_{\mathrm{Loss}} = \frac{1}{\Lambda^2/D_X + 2(\pi R^2 L)(2-\gamma)/S v_{\mathrm{th}} \gamma}, \tag{10}$$

where D_X is the neutral diffusion coefficient, γ the sticking coefficient on the wall, S the surface area of the chamber, v_{th} the thermal velocity, and the effective diffusion length Λ is given by

$$\Lambda^{-2} = \left(\frac{\pi}{L}\right)^2 + \left(\frac{2.405}{R}\right)^2.$$

On the other hand, the diffusional losses of positive ions to the wall are also estimated, as shown in previously published papers.[30,31] The density $n_e(=n_+)$ falls relatively abruptly near the sheaths to edge values $n_{e\ell}=h_l n_e$ and $n_{er}=h_r n_e$ at the axial and circumferential sheaths, where the velocity for positive

TABLE II. Main reaction set for hydrogen.

Reaction	Rate coefficient ($m^3\ s^{-1}$)	Ref.
$H+e \rightarrow H(2p)+e$	$k_{14}=2.1\times10^{-14}\exp(-10.67/T_e)$	35
$H+e \rightarrow H(2s)+e$	$k_{15}=5.0\times10^{-15}\exp(-9.0/T_e)$	35
$H(2s)+e \rightarrow H(2p)+e$	$k_{16}=3.5\times10^{-12}$	35
$e+H \rightarrow H^+ +2e$	$k_{17}=1.75\times10^{-14}\exp(-15.4/T_e)$	35
$e+H(2s) \rightarrow H^+ +2$	$k_{18}=1.97\times10^{-13}\exp(-4.43/T_e)$	35
$e+H_2 \rightarrow H+H+e$	$k_{19}=1.2\times10^{-14}\exp(-10/T_e)$	35
$e+H_2 \rightarrow H+H(2s)+e$	$k_{20}=4.71\times10^{-15}\exp(-15.9/T_e)$	35
$e+H_2 \rightarrow H(2p)+H(2s)+e$	$k_{21}=1.78\times10^{-15}\exp(-28.34/T_e)$	35
$e+H_2 \rightarrow H+H(n=3)+e$	$k_{22}=3.74\times10^{-16}\exp(-18.0/T_e)$	35
$e+H_2 \rightarrow H_2^+ +2e$	$k_{23}=3.11\times10^{-14}\exp(-18.9/T_e)$	35 and 36
$e+H_2 \rightarrow H+H^+$	$k_{24}=3.07\times10^{-16}\exp(-17.5/T_e)$	35
$e+H_2^+ \rightarrow H+H(n\geq2)$	$k_{25}=8.0\times10^{-14}\exp(-0.2T_e)$	35
$e+H_2^+ \rightarrow H^+ +H+e$	$k_{26}=1.45\times10^{-13}\exp(-1.97/T_e)$	35
$e+H_3^+ \rightarrow H_2+H$	$k_{27}=1.55\times10^{-13}(300/T_g)$	17
$H_2+H_2^+ \rightarrow H_3^+ +H$	$k_{28}=2.1\times10^{-15}$	26
$H(2p) \rightarrow H+h\nu$	$4.7\times10^7\ (s^{-1})$	27
$H^+ \rightarrow H$ (wall loss)	$H^+_{Loss}=2U_{B,H}(R^2h_\ell+RLh_r)/R^2L\ s^{-1}$	
$H_2^+ \rightarrow H_2$ (wall loss)	$H^+_{2Loss}=2U_{B,H_2}(R^2h_\ell+RLh_r)/R^2L\ s^{-1}$	
$H_3^+ \rightarrow H+H_2$ (wall loss)	$H^+_{3Loss}=2U_{B,H_3}(R^2h_\ell+RLh_r)/R^2L(s^{-1})$	
$H \rightarrow \frac{1}{2}H_2$ (wall loss)	$H_{Loss}=(\Lambda^2/D_H+2\pi R^2L(2-\gamma)/Sv_{th}\gamma)^{-1}\ (s^{-1})$ ($\gamma=0.02$)	
$H(2s) \rightarrow H$ (wall loss)	$D_{m,H}/\Lambda^2$	

ion X^+ can reach the Bohm velocity U_{B,X_p}. The h_l and h_r factors are expressed as[30]

$$h_l=\frac{0.86}{\sqrt{3+\frac{L}{2\lambda_i}}}, \tag{11}$$

and

$$h_r=\frac{0.8}{\sqrt{4+\frac{R}{\lambda_i}}}. \tag{12}$$

The mean free path λ_i in Ar/H_2 is given by

$$\frac{1}{\lambda_i}=[Ar]\sigma_{Ar}+[H]\sigma_H+[H_2]\sigma_{H_2},$$

where σ_{Ar}, σ_H, and σ_{H_2} correspond to the total ion-neutral collision cross sections.[22,31] Then, the diffusional losses X^+_{Loss} of positive ions X^+ (X=Ar, ArH, H, H_2, and H_3) to the wall is given by

TABLE III. Reaction set for interactions between hydrogen and argon.

Reaction	Rate coefficient ($m^3\ s^{-1}$)	Ref.
$Ar_m+H_2 \rightarrow Ar+H+H$	$k_{29}=1.1\times10^{-16}$	27
$Ar_r+H_2 \rightarrow Ar+H+H$	$k_{30}=1.1\times10^{-16}$	27
$Ar^+ +H_2 \rightarrow Ar+H_2^+$	$k_{31}=8\times10^{-17}$	26
$Ar^+ +H_2 \rightarrow H+ArH^+$	$k_{32}=6\times10^{-16}$	26
$ArH^+ +H_2 \rightarrow H_3^+ +Ar$	$k_{33}=1.5\times10^{-15}$	26
$ArH^+ +e \rightarrow Ar+H$	$k_{34}=1.7\times10^{-13}$	26
$ArH^+ \rightarrow Ar+H$ (wall loss)	$ArH^+_{Loss}=2U_{B,ArH}(R^2h_\ell+RLh_r)/R^2L\ (s^{-1})$	

$$X^+_{Loss}=2U_{B,X_p}(R^2h_l+RLh_r)/R^2L. \tag{13}$$

The energy balance equation assumes that all power injected into the plasma is dissipated through collision processes between electrons and neutral species and the kinetic energies of ions and electrons flowing into the walls. The energy balance equation in Ar/H_2 plasma is given by

$$\frac{3}{2}\frac{d(en_eT_e)}{dt}=\frac{P_{abs}}{\pi R^2L}-\sum e\mathcal{E}_c^{(X)}k_{iz,X}[X]n_e-e(\mathcal{E}_e+\mathcal{E}_i)\sum[X_p^+]X^+_{p,Loss}, \tag{14}$$

where $\mathcal{E}_c^X$ is the collisional energy loss per electron-ion pair created for the neutral X (X=Ar, H, and H_2), which includes all excitation energies such as vibrational, dissociative, and electronic excitations.[32–36] The energy $\mathcal{E}_i$, which corresponds to the energy lost to ions accelerating through the sheath, is given by $\mathcal{E}_i=eV_{sh}+T_e/2$ since the ion bombarding energy reaches the sum of the ion energy entering the sheath and the energy gained in the sheath. The sheath edge voltage drop V_{sh} is given as $V_{sh}=(T_e/2e)\ln(M_{eff}/2\pi m)$. On the other hand, the energy $\mathcal{E}_e$ corresponding to the electron energy lost to the walls is given by $\mathcal{E}_e=2T_e$. The equations for each particle and power balance are then solved by the Runge–Kutta numerical method to obtain an equilibrium.

As is described above, the global model for electropositive plasma is used in this paper. The electronegativity α can be estimated from the particle balance equation for H^-. The dominant production of H^- is due to the dissociative attachment collisions between the vibrationally excited hydrogens $H_2(v)$ of level v ($v\geq4$) and electrons,[35,37] whereas the dominant loss of H^- should be due to the detachment collisions between H^- and H as well as recombination process between

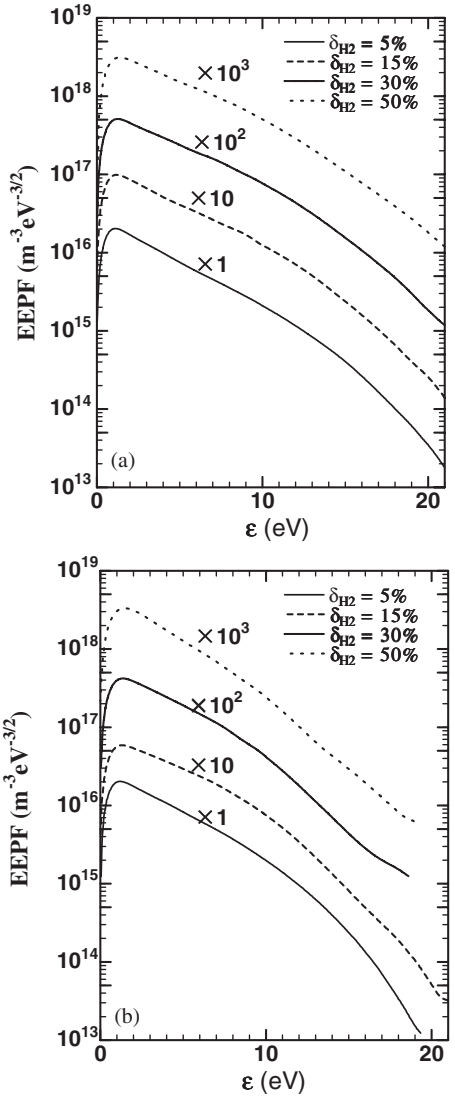

FIG. 2. EEPFs measured in Ar/H_2 discharges at (a) $p=20$ mTorr and (b) $p=60$ mTorr, where $P_{abs}=120$ W.

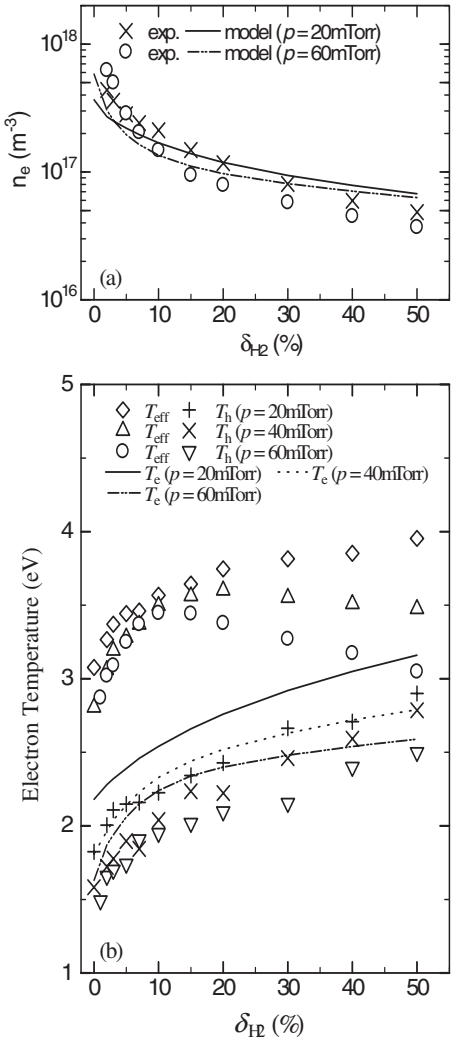

FIG. 3. (a) Electron density and (b) electron temperatures as a function of hydrogen fraction.

positive and negative ions. When the dominant loss of H^- is assumed to be due to the detachment process for simplicity, the ratio α is given as

$$\alpha = C_{ad}\frac{n_{H_2(v)}}{n_H},$$

where C_{ad} is the ratio of rate coefficient for the dissociative attachment to that for detachment and $n_{H_2(v)}$ is the density of $H_2(v)$ of level $v(v \geq 4)$. The density ratio $n_{H_2(v)}(v \geq 4)/n_{H_2}$ is much lower than 10^{-3}–10^{-4}, as is reported in the previous papers.[21,37] On the other hand, the ratio n_H/n_{H_2} is expected to be higher than 0.01. The ratio of $n_{H_2(v)}$ to n_H is on the order of 10^{-2} and the estimated value of C_{ad} is less than 5–10.[21,35,37] Thus, the value of α is much lower than 1, so that the negative ions are not considered in the model.

IV. RESULTS AND DISCUSSION

The EEPFs measured at $p=20$ m and 60 mTorr are given in Figs. 2(a) and 2(b). The EEPFs measured at any condition slightly deviate from the Maxwellian distribution owing to the depletion of electrons, which have an enough energy to cause the electronic excitation collisions with the neutral species. Thus, we can approximate the distribution by exponentials in the bulk with a slope $1/T_b$ and above the energy ε_{knee} at the knee point with a slope $1/T_h$. The energy ε_{knee} decreases from about 11–13 eV corresponding to the lowest excitation threshold energy of Ar to about 8–9 eV corresponding to the lowest electronic excitation threshold energy of H_2, with increasing δ_{H_2}. The ratios $R_{Ar,H}$ and $R_{H_2,H}$ can be determined using the measured T_h rather than the measured T_b. The temperature T_b, which is approximately equal to T_{eff}, is higher than T_h by about 1.0–2.0 eV. The difference between T_{eff} and T_h decreases as δ_{H_2} increases. Therefore, the EEPF structure can be gradually changed from being Druyvesteyn-type to being Maxwellian-type by increasing only δ_{H_2}.

In Figs. 3(a) and 3(b), the electron density and its temperatures are shown as a function of δ_{H_2}, together with the calculation results of the model. The measured and calculated n_e markedly decrease with increasing δ_{H_2} at δ_{H_2} lower than 10%–20%. The marked decrease in n_e with increasing δ_{H_2} is more prominent as the total pressure increases. The

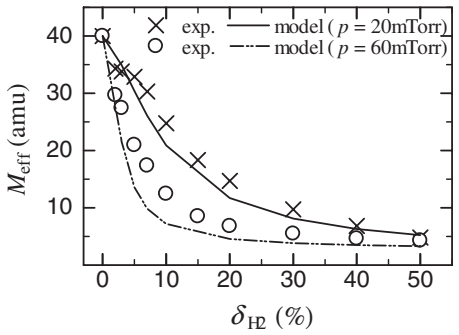

FIG. 4. Effective ion mass as a function of hydrogen fraction.

measured T_{eff} and T_h relatively abruptly increase with increasing δ_{H_2} until δ_{H_2} reaches 10%. For δ_{H_2} higher than 10%, the temperature T_h gradually increases with the increase in δ_{H_2}, whereas the relationship between T_{eff} and δ_{H_2} depends on the total pressure. The calculated electron temperature T_e also relatively abruptly increases until δ_{H_2} reaches approximately 10%, beyond which it gradually increases. As is expected, the calculated T_e is close to T_h rather than T_{eff} because the high-temperature portion of the distribution dominates the calculated temperature, which is determined mainly from the exponentially temperature-sensitive ionization rate.

In Fig. 4, the effective ion mass M_{eff} in the Ar/H_2 plasmas, which should be estimated using Eq. (8), is shown as a function of δ_{H_2}. In addition, the results of the model, in which the calculated densities of all positive ion species are used under the assumption that all positive ion species have a same profile even in the vicinity of the probe sheath, are also shown. The ions in Ar/H_2 plasmas are classified into the group of heavy ions, such as Ar^+ and ArH^+, and that of light ions, such as H^+, H_2^+, and H_3^+. The large difference between masses of two groups can help us in deducing the ion compositions in the plasma and in understanding the effect of the interactions between Ar ions and neutral hydrogens. As is shown in Fig. 4, reasonable agreement between the experiment and the model is obtained, and those results show that the effective ion mass markedly decreases from 40 (the mass of Ar^+) to about three (the mass of H_3^+). From the marked decrease in n_e and M_{eff} with the increase in δ_{H_2}, it can be predicted that the densities of Ar^+ and ArH^+ markedly decreasing with increasing δ_{H_2}, and the hydrogen ions $H_x^+(x=3,2)$ are predominant even at $\delta_{H_2} \approx 15-20\%$, beyond which the densities of the hydrogen ions $H_x^+(x=3,2)$, which are approximately equal to n_e, gradually decrease with increasing δ_{H_2}.

The ratios $R_{Ar,H}$ and $R_{H_2,H}$ are necessary in order to calculate the density of hydrogen atoms from Eq. (9). The ratios should be calculated using the measured EEPFs and the corresponding cross sections.[38–41] Figures 5(a) and 5(b) show $R_{Ar,H}$ and $R_{H_2,H}$ calculated as a function of δ_{H_2}. The ratio $R_{Ar,H}$ does not strongly depend on T_h, whereas the ratio $R_{H_2,H}$, which is much smaller than $R_{Ar,H}$, depends on T_h. The dependence of n_H on δ_{H_2} for various p is shown in Fig. 6. The calculated density of hydrogen atoms shows reasonable agreement with n_H estimated using actinometry, although

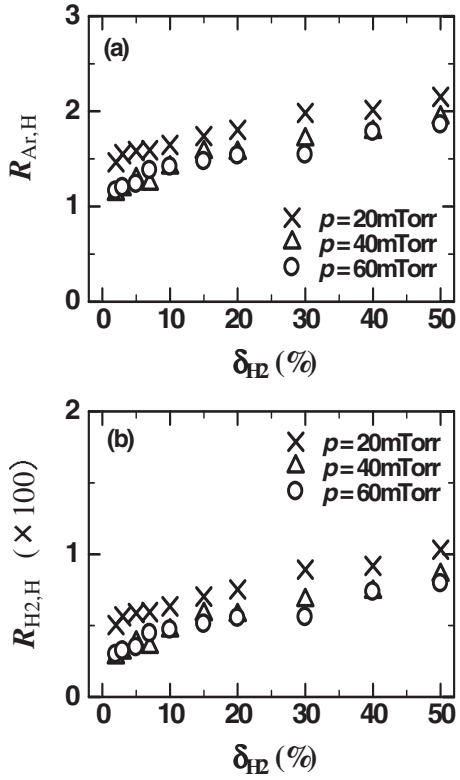

FIG. 5. Estimated values of (a) $R_{Ar,H}$ and (b) $R_{H_2,H}$.

there still remains significant difference at δ_{H_2} lower than 10%. The density n_H markedly increases as hydrogen is added to the Ar discharges, and then saturate at δ_{H_2} of 20–30%. The calculated density of hydrogen atoms can correspond to the density of the ground-state hydrogen atoms because the densities of H(2*s*) and H(2*p*) atoms are lower than the density of the ground-state hydrogen atoms by three to four orders of magnitude. Although we used γ value of 0.02 for hydrogen atoms, we found that n_H is approximately proportional to the inverse of γ value, which should strongly depend on various factors related to the surface conditions of the chamber. However, the reasonable agreement of magnitude of measured and calculated n_H indicate that γ value used in the model may agree with the true value within a factor of 2–3. As shown in Fig. 7, the calculated degree of dissociation, which is defined as $n_H/(n_H+2n_{H2})$, decreases

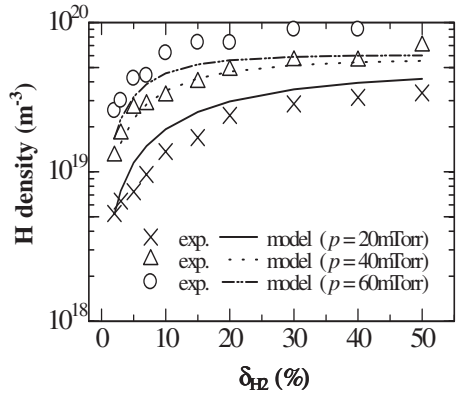

FIG. 6. Comparison of calculated density of hydrogen atoms with experimental one, where T_g is assumed to be 400 K.

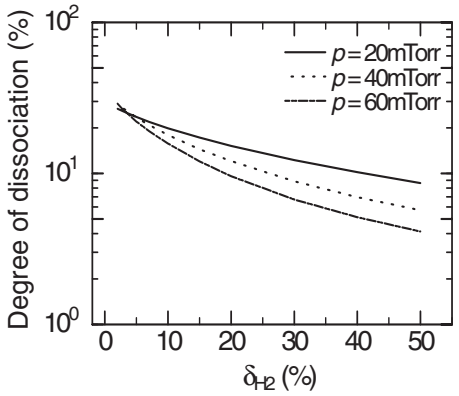

FIG. 7. Degree of dissociation calculated as a function of hydrogen fraction.

from 30% at $\delta_{H_2}=3\%$ to 9% at $\delta_{H_2}=50\%$ for $p=20$ mTorr, from 30% at $\delta_{H_2}=3\%$ to 4% at $\delta_{H_2}=50\%$ for $p=60$ mTorr, with increasing δ_{H_2}.

The model results are compared with the experiments, obtaining reasonably good agreement for the measurable parameters described above. Thus, the relationships between the other plasma parameters and δ_{H_2} should be explained using the model. Aside from the hydrogen atoms, the Ar metastables and resonants in the neutral species may also play a significant role on the determination of the plasma compositions due to the interactions such as quenching collisions. Figure 8 shows the density of Ar metastables calculated as a function of δ_{H_2}. Here, the density of Ar metastables corresponds to the sum of densities of Ar atoms excited to the levels $1s^5$ and $1s^3$. The density of Ar resonant is omitted in this paper because the difference between the density of Ar matastables and that of Ar resonants is small. The calculated density of the metastables slightly increases due to the marked increase in excitation collision frequency at a small addition of hydrogen lower than 3%, beyond which it decreases with increase in δ_{H_2} due to the quenching collisions with the molecular hydrogens. The quenching collisions between Ar metastables and molecular hydrogens may play a significant role on the production of hydrogen atoms because the frequency of the quenching collisions may be comparable to that of H_2 dissociation by the electron impact.

The calculated positive ion densities are, respectively, shown in Figs. 9(a) and 9(b) at $p=20$ m and 60 mTorr. The density of Ar^+ markedly decreases with the increase in the

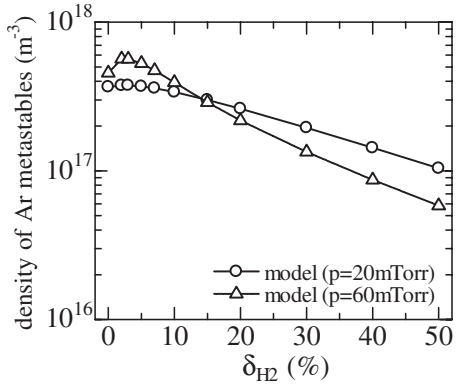

FIG. 8. Density of Ar metastables calculated in the model.

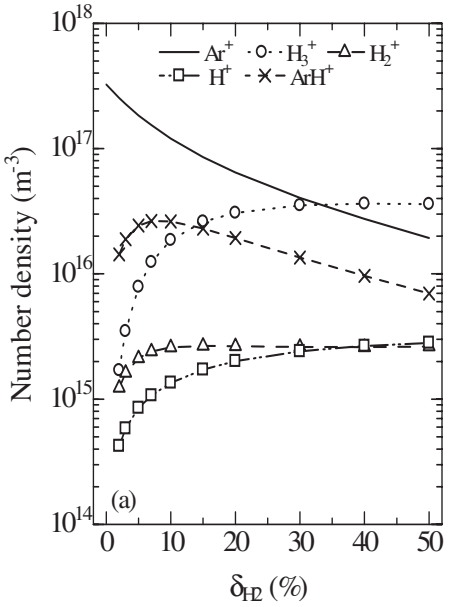

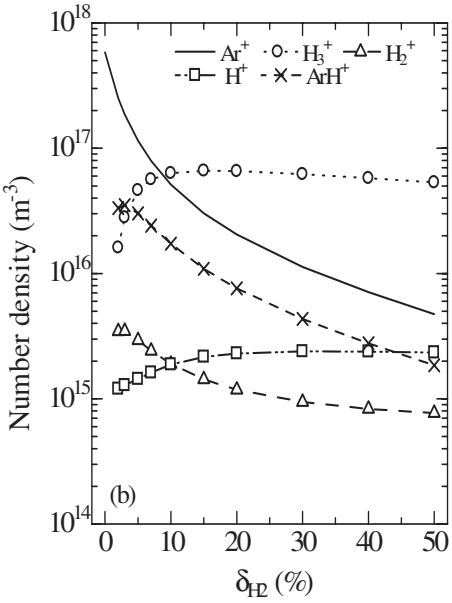

FIG. 9. Positive ion densities calculated in Ar/H_2 discharges at (a) $p=20$ mTorr and (b) $p=60$ mTorr.

hydrogen fractions owing to the charge exchange collisions between Ar^+ and molecular hydrogens. The decrease in Ar^+ density is more prominent as p increases. On the other hand, the density of H_3^+ relatively abruptly increases at the hydrogen fractions of approximately 10%–20% and then does not strongly depend on the hydrogen fractions. The change of the predominant ion species from Ar^+ to H_3^+ can be occurred at lower hydrogen fractions as the total pressure increases. The density of ArH^+ ions abruptly increases at the hydrogen fractions lower than 5%–10%, and then gradually decreases with the increase in the hydrogen fraction. The densities of $H_x(x=1,2)$ ions are not sensitive to the hydrogen fraction at the fractions higher than 15%–20%.

It has been experimentally reported that the flux ratio of H^+ to H_2^+ is small and that of H_3^+ to H_2^+ is almost equal in inductive Ar/H_2 plasmas, predicting that H_2^+ density, which is much larger than H^+ density, is comparable to that of

H_3^+.[42,43] Such tendency differs from the model results, although the experimental conditions are not same as the calculation ones. The calculated density of H_2^+ strongly depends on the value of rate coefficient k_{28}, whereas that of H_3^+ does not strongly depends on the value of k_{28}. The density ratio of H_3^+ to H_2^+ is approximately proportional to the inverse of k_{28}. The value of k_{28}, which should depend on ion temperature or ion energy,[35] may be overestimated because we assume that the ion temperature is equal to the gas temperature. As is predicted from the dependence of n_H on γ value, the calculated densities of H^+ is also approximately proportional to the inverse of γ. Reasonable agreement between the experiments[42,43] and the model may be obtained when the values of k_{28} and γ are appropriately estimated according to respective experimental conditions. Further experimental and theoretical investigations on the properties of hydrogen containing discharges will be required.

However, we can conclude that the addition of Ar to the hydrogen discharges is very useful to easily produce the stable plasmas, keeping the densities of H_x ions as well as the density of hydrogen atoms over the wide range of Ar dilution.

V. CONCLUDING REMARKS

Experiments with a Langmuir probe and optical emission spectroscopy combined with actinometry were carried out in inductive Ar/H_2 discharges at three total pressures of 20 m, 40 m, and 60 mTorr for hydrogen fractions ranging from 0% to 50%. The measured EEPFs deviate from the Maxwellian distributions owing to the depletion of high-energy electrons and can be approximated by using two temperatures. The measured electron density decreases with increasing the hydrogen fraction in the hydrogen fraction below 20%, beyond which it gradually increases. On the other hand, the temperatures relatively abruptly increase with increasing the hydrogen fraction in the hydrogen fractions below 10%. The effective ion mass, which was estimated a by the ion current collected into the probe, markedly decreases with the increase in the hydrogen fraction, indicating that the dominant positive ion is H_3^+ even at the hydrogen fractions lower than 15%–20%. The density of hydrogen atoms estimated by actinometry markedly increases as hydrogen is added to Ar discharges, and then gradually increases with increasing the hydrogen fraction at the hydrogen fractions higher than 10%–20%.

A global model is used to study the effect of hydrogen addition to Ar discharges on the plasma parameters assuming the Maxwellian electron energy distribution. Experimental results described above were compared with the results of global model, and the reasonably good agreement was obtained. Some of the model results are summarized as follows:

(1) The density of Ar^+ markedly decreases with the increase in the hydrogen fractions owing to the charge exchange collisions between Ar^+ and molecular hydrogens, whereas that of H_3^+ relatively abruptly increases at the hydrogen fractions of approximately 10%–20% and then does not strongly depend on the hydrogen fractions. The change of the predominant ion species from Ar^+ to H_3^+ can be occurred at lower hydrogen fractions as the total pressure increases. The density of ArH^+ ions abruptly increases at the hydrogen fractions lower than 5%–10%, and then gradually decreases with the increase in the hydrogen fraction. The densities of $H_x(x=1,2)$ ions are not sensitive to the hydrogen fraction at the fractions higher than 15%–20%.

(2) The density of hydrogen atoms markedly increases as hydrogen is added to Ar discharges, and then gradually increases with increasing the hydrogen fraction at the hydrogen fractions higher than 10%–20%.

In conclusion, the addition of Ar to the hydrogen discharges is very useful to easily produce the stable plasmas, keeping the densities of H_x $(x=1-3)$ ions as well as density of hydrogen atoms over wide range of Ar dilution.

[1] P. K. Bachmann, D. Leers, and H. Lyatin, Diamond Relat. Mater. **1**, 1 (1991).
[2] R. A. Gottscho, B. L. Preppernau, S. J. Pearton, A. B. Emerson, and K. P. Giappis, J. Appl. Phys. **68**, 440 (1990).
[3] T. P. Schneider, J. Cho, Y. L. Chen, D. M. Maher, and R. J. Nemanich, *Surface Chemical Cleaning and Passivation for Semiconductor Processing*, MRS Symposia Proceedings No. 315 (Materials Research Society, Pittsburgh, 1993), p. 197.
[4] A. Gicquel, E. Anger, M. F. Ravet, D. Fabre, D. Scatena, and Z. Z. Wang, Diamond Relat. Mater. **2**, 417 (1993).
[5] C. Findeling-Dufour, A. Gicquel, and R. Chiron, Diamond Relat. Mater. **7**, 986 (1998).
[6] E. Vallat-Sauvain, U. Kroll, J. Meier, A. Shah, and J. Pohl, J. Appl. Phys. **87**, 3137 (2000).
[7] M. Kondo, M. Fukawa, L. Gou, and A. Matsuda, J. Non-Cryst. Solids **266-269**, 84 (2000).
[8] A. Grill, A. V. Sternhagen, D. Neumayer, and V. Patel, J. Appl. Phys. **98**, 074502 (2005).
[9] B. P. Lavrov, A. V. Pipa, and J. Ropcke, Plasma Sources Sci. Technol. **15**, 135 (2006).
[10] B. P. Lavrov, N. Lang, A. V. Pipa, and J. Ropcke, Plasma Sources Sci. Technol. **15**, 147 (2006).
[11] M. Abdel-Rahman, V. Schulz-von der Gathen, T. Gans, K. Niemi, and H. F. Dobele, Plasma Sources Sci. Technol. **15**, 620 (2006).
[12] J. Loureiro and C. M. Ferreira, J. Phys. D **22**, 1680 (1989).
[13] A. Garscadden and R. Napgal, Plasma Sources Sci. Technol. **4**, 268 (1995).
[14] J. Amorim, J. Loureiro, G. Baravian, and M. Touzeau, J. Appl. Phys. **82**, 2795 (1997).
[15] B. F. Gordiets, C. M. Ferreira, M. J. Pinheiro, and A. Ricard, Plasma Sources Sci. Technol. **7**, 363 (1998).
[16] K. Hassouni, A. Gicquel, M. Capitelli, and J. Loureiro, Plasma Sources Sci. Technol. **8**, 494 (1999).
[17] B. Gordiets, M. Pinheiro, E. Tatarova, F. M. Dias, C. M. Ferreira, and A. Ricard, Plasma Sources Sci. Technol. **9**, 295 (2000).
[18] M. Capitelli, R. Celiberto, F. Esposito, A. Laricchiuta, K. Hassouni, and S. Longo, Plasma Sources Sci. Technol. **11**, A7 (2002).
[19] A. Salabas, L. Marques, J. Jolly, G. Gousset, and L. L. Alves, J. Appl. Phys. **95**, 4605 (2004).
[20] P. Diomede, M. Capitelli, and S. Longo, Plasma Sources Sci. Technol. **14**, 459 (2005).
[21] L. Marques, J. Jolly, and L. L. Alves, J. Appl. Phys. **102**, 063305 (2007).
[22] R. Zorat, J. Goss, D. Boilson, and D. Vender, Plasma Sources Sci. Technol. **9**, 161 (2000).
[23] M. A. Lieberman and R. A. Gottscho, in *Physics of Thin Films* edited by M. Francombe and J. Vossen, (Academic, New York, 1994), Vol. 18, p. 1.
[24] C. Lee, D. B. Graves, M. A. Lieberman, and D. W. Hess, J. Electrochem. Soc. **141**, 1546 (1994).
[25] C. Lee and M. A. Lieberman, J. Vac. Sci. Technol. A **13**, 368 (1995).
[26] N. Laidani, R. Bartali, P. Tosi, and M. Anderle, J. Phys. D **37**, 2593 (2004).
[27] F. J. Gordillo-Vázquez and J. M. Albella, J. Appl. Phys. **94**, 6085 (2003).

[28]M. J. Druyvesteyn, Z. Phys. **64**, 781 (1930).
[29]T. Kimura and K. Ohe, Plasma Sources Sci. Technol. **8**, 553 (1999).
[30]V. A. Godyak, *Soviet Radio Frequency Discharge Research* (Delphic Associates, Falls Church, VA, 1986).
[31]M. A. Lieberman and A. J. Lichtenberg, *Principles of Plasma Discharges and Materials Processing*, 2nd ed. (Wiley, New York, 2005).
[32]J. T. Gudmundsson and E. G. Thorsteinsson, Plasma Sources Sci. Technol. **16**, 399 (2007).
[33]T. Kimura and T. Takai, Jpn. J. Appl. Phys., Part 1 **43**, 7240 (2004).
[34]T. Kimura and K. Ohe, J. Appl. Phys. **89**, 4240 (2001).
[35]R. K. Janev, W. D. Langer, K. Evans, Jr., and D. E. Post, Jr., *Elementary Processes in Hydrogen-Helium Plasmas* (Springer-Verlag, New York, 1987).
[36]H. Tawara, Y. Itikawa, H. Nishimura, and M. Yoshino, J. Phys. Chem. Ref. Data **19**, 617 (1990).
[37]W. G. Graham, Plasma Sources Sci. Technol. **4**, 281 (1995).
[38]J. D. Walker, Jr. and R. M. St John, J. Chem. Phys. **61**, 2394 (1974).
[39]G. R. Möhlmann, F. J. DeHeer, and L. Los, Chem. Phys. **25**, 103 (1977).
[40]M. V. Malyshev and V. M. Donnelly, J. Vac. Sci. Technol. A **15**, 550 (1997).
[41]U. Fanz, Plasma Sources Sci. Technol. **15**, S137 (2006).
[42]J. T. Gudmundsson, Plasma Sources Sci. Technol. **7**, 330 (1998).
[43]J. T. Gudmundsson, Plasma Sources Sci. Technol. **8**, 58 (1999).